Molecular and Clinical Stratification of Astroblastomas: Three Distinct Fusion-Defined Groups Informing Risk-Adapted Treatment Strategies

Aniello Federico[1,2,3*], Felix Schmitt-Hoffner[1,2,3,4*], Adriana Fonseca[5*], Neal Geisemeyer[1,2,3], Katharina Bruckner[6], Monika Mauermann[1,2,3], Martin Sill[1,2,7], Damian Stichel[8], Dominik Sturm[1,3,8,10], Ulrich Schüller[11,12,13], Arnault Tauziede-Espariat[14], Pascale Varlet[14], David Capper[6,15], Zied Abdullaev[16], Daniel Schrimpf[7], Florian Selt[1,3,8], Lane Williamson[5], Andrew M. Donson[17], Manila Antonelli[18,19], Evelina Miele[20], Matija Snuderl[21], Sebastian Brandner[22], Maria Łastowska[23], Jasper van der Lugt[24], Jens Bunt[24], Christof Kramm[25], Alexandra Kolenova[26], Aditya Raghunathan[27], Yelena Wilson[28], Lauren Weintraub[29], Jordan R. Hansford[30,31], Sabine Spiegl-Kreinecker[32], Barbara Aistleitner[33], Lorena Baroni[34], Michal Zapotocky[35], Vijay Ramaswamy[36], Andrey Korshunov[7], Barbara Jones[1,3,8,9], Mimi Kjaersgaard[37], Mariëtte E. Kranendonk[24], Christine Haberler[38], Roger J. Packer[5,39], Natalie Jäger[1,2,3], Andreas von Deimling[1,3,7], Felix Sahm [1,3,7], Jan Koster[40], Kenneth Aldape[16], Stefan M. Pfister[1,2,3,8], Katja von Hoff[41,42,#], Johannes Gojo [13,#], Marcel Kool[1,2,3,23,43,#]

1. Hopp-Children's Cancer Center Heidelberg (KiTZ), Heidelberg, Germany
2. Division of Pediatric Neurooncology, German Cancer Research Center (DKFZ) and German Cancer Consortium (DKTK), Heidelberg, Germany
3. Department of Pediatric Hematology and Oncology, Heidelberg University Hospital, and National Center for Tumor Diseases (NCT), Heidelberg, Germany
4. Faculty of Biosciences, Heidelberg University, Heidelberg, Germany
5. Brain Tumor Institute, Children's National Medical Center, 111 Michigan Avenue NW, Washington, DC, 20010, USA
6. Department of Pediatrics and Adolescent Medicine, Comprehensive Cancer Center and Comprehensive Center for Pediatrics, Medical University of Vienna, Vienna, 1090, Austria
7. German Cancer Consortium (DKTK), Partner Site Berlin, German Cancer Research Center (DKFZ), Heidelberg, Germany
8. Department of Neuropathology, Heidelberg University Hospital, Heidelberg, Germany
9. Division of Pediatric Glioma Research, German Cancer Research Center (DKFZ) and German Cancer Consortium (DKTK), Heidelberg, Germany
10. Department of Pediatric Oncology, Hematology & Immunology, Heidelberg University Hospital, Heidelberg, Germany
11. Department of Pediatric Hematology and Oncology, University Medical Center Hamburg-Eppendorf, Hamburg, Germany
12. Institute of Neuropathology, University Medical Center Hamburg-Eppendorf, Hamburg, Germany
13. Research Institute Children's Cancer Center Hamburg, Hamburg, Germany
14. Department of Neuropathology, GHU Paris Psychiatry and Neurosciences, Sainte-Anne Hospital, Paris, France
15. Department of Neuropathology, Charité Universitätsmedizin Berlin, Berlin, Germany
16. Laboratory of Pathology, Center for Cancer Research, National Cancer Institute, National Institutes of Health, Bethesda, MD, USA

17. Morgan Adams Foundation Pediatric Brain Tumor Research Program, Department of Pediatrics, University of Colorado School of Medicine, Aurora, CO, USA
18. Department of Radiological, Oncological and Anatomic Pathology, Sapienza University, Rome, Italy.
19. IRCCS Istituto Neurologico Mediterraneo NEUROMED, Via Atinense 18, 86077 Pozzilli, Italy
20. Onco-Hematology, Cell Therapy, Gene Therapies and Haemopoietic Transplant, Bambino Gesù Children's Hospital, IRCCS, Rome, Italy
21. Department of Pathology, New York University School of Medicine, New York, NY, USA
22. Department of Neurodegeneration, Institute of Neurology, University College London, London, UK
23. Department of Pathomorphology, the Children's Memorial Health Institute, Warsaw, Poland
24. Princess Máxima Center for Pediatric Oncology, Utrecht, the Netherlands
25. Division of Pediatric Hematology and Oncology, University Medical Center Goettingen, Goettingen, Germany
26. Comenius University Children's Hospital Limbova 1, Bratislava, Slovakia
27. Department of Laboratory Medicine and Pathology, Mayo Clinic, Rochester, Minnesota, USA
28. Department of Pathology, Akron Children's Hospital, Akron, OH, USA
29. Pediatric Hematology/Oncology, Albany Medical Center, Albany, New York, USA
30. Children's Cancer Centre, Royal Children's Hospital; Murdoch Children's Research Institute; Department of Pediatrics, University of Melbourne, Melbourne, Victoria, Australia
31. Michael Rice Center for Haematology and Oncology, Women's and Children's Hospital; South Australia Health and Medical Research Institute; South Australia ImmunoGENomics Cancer Institute, University of Adelaide, Adelaide, SA, Australia
32. Department of Neurosurgery, Kepler University Hospital GmbH, Johannes Kepler University, Linz, Austria
33. Department of Pediatrics and Adolescent Medicine, Johannes Kepler University Linz, Linz, Austria
34. Department of Hematology/Oncology, Hospital JP Garrahan, Combate de los Pozos 1881, Buenos Aires, Argentina
35. Prague Brain Tumor Research Group, Second Faculty of Medicine, Charles University and University Hospital Motol, Prague, Czech Republic
36. Division of Haematology/Oncology and Department of Paediatrics, Hospital for Sick Children, Toronto, Canada
37. Department of Paediatrics and Adolescent Medicine, Children and Adolescents with Cancer and Hematological Diseases, Rigshospitalet, Copenhagen, Denmark
38. Division of Neuropathology and Neurochemistry, Department of Neurology, Medical University of Vienna, Vienna, Austria
39. Center for Neuroscience and Behavioral Medicine, Children's National Medical Center, 111 Michigan Avenue NW, Washington, DC, 20010, USA
40. Center for Experimental and Molecular Medicine, Laboratory of Experimental Oncology and Radiobiology, Cancer Center Amsterdam, Amsterdam UMC, University of Amsterdam, Amsterdam, the Netherlands
41. Charité – Universitätsmedizin Berlin, corporate member of Freie Universität Berlin and Humboldt-Universität zu Berlin, Berlin, Germany
42. Department of Paediatric and Adolescent Medicine, Aarhus University Hospital, Aarhus, Denmark
43. University Medical Center Utrecht, Utrecht University, Utrecht, the Netherlands

*Aniello Federico, Felix Schmitt-Hoffner and Adriana Fonseca contributed equally to this work.

# Marcel Kool, Johannes Gojo and Katja von Hoff contributed equally to this work.

Running title: Molecular and Clinical Stratification of Astroblastomas

Corresponding authors:

Marcel Kool; Princess Máxima Center for Pediatric Oncology, Utrecht, the Netherlands; m.kool-5@prinsesmaximacentrum.nl

Johannes Gojo; Department of Pediatrics and Adolescent Medicine, Medical University of Vienna, Vienna, 1090, Austria; johannes.gojo@meduniwien.ac.at

Abstract

Background: Astroblastomas are rare brain tumors predominantly affecting children and young adults, for which molecular subtypes and clinical management remain undefined.

Methods: We analyzed tumor samples, molecular profiles, and clinical data from 200 patients, classified as “Astroblastoma, *MN1*-altered” under WHO criteria, using DNA methylation profiling, DNA/RNA profiling/sequencing, and survival analyses.

Results: DNA methylation analyses identified three groups: Group A (n=143, characterized by *MN1::BEND2* fusions, predominantly supratentorial location, with striking female predominance and favorable survival); Group B (n=37, epigenetically and transcriptionally closely related to Group A, but characterized by *EWSR1::BEND2* fusions, with spinal and infratentorial locations and poor prognosis); and Group C (n=20, epigenetically and transcriptionally distinct, characterized by *MN1::CXXC5* fusions, exclusively supratentorially located, with favorable survival). Progression-free and overall survival were significantly shorter in Group B (5-year PFS 14%; 10-year OS 54%) compared to A (5-year PFS 47%; 10-year OS 89%) and C (5-year PFS 75%; 10-year OS 89%). Radiotherapy improved PFS in Group B (hazard ratio 0.25), while no clear benefit was identified for Group A and C.

Conclusions: Astroblastoma, *MN1*-altered, comprises three molecularly and clinically distinct groups, characterized by different fusion genes, including those without *MN1*. These new insights, including identification of potential predictive biomarkers like 14q/16q loss, provide a framework for development of risk-stratified therapeutic approaches. Importantly, we identified a molecularly defined high-risk group that benefits from radiation therapy. Our findings redefine Astroblastoma as a molecularly diverse tumor type, propose a refined classification, support the development of risk-adapted therapeutic strategies and provide a rational standard of care.

Key words

Astroblastoma, *MN1*-altered; *MN1::BEND2; MN1::CXXC5; EWSR1::BEND2*; gene fusion.

Key points

Astroblastoma, MN1-altered, comprises three molecularly and clinically distinct subgroups

Gene fusions, including ones without MN1, define astroblastoma subgroups

Different clinical outcomes and therapeutic effects suggest diverse therapeutic strategies

Importance of the study

This study is the first to provide a comprehensive overview of the molecular and clinical landscape of 'Astroblastoma, *MN1*-altered', a novel brain tumor type introduced in the latest WHO classification of central nervous system tumors. Molecular analyses identified three related groups, characterized by distinct *MN1* (fused to either *BEND2* or *CXXC5*) or *BEND2* (fused mainly but not restricted to *EWSR1*) fusions. We therefore propose to rename this group into Astroblastoma. Importantly, we uncover group-specific clinical and therapeutic differences, and risk factors, all directly relevant for future clinical management. Furthermore, we provide evidence that Group B tumors, mainly characterized by *EWSR1::BEND2* fusions, are associated with a poor outcome, but these patients may benefit from radiotherapy. In addition,

molecular analyses provide first therapeutic leads for targeted therapies. Accordingly, our study of the largest astroblastoma cohort published to date provides essential guidance for current treatment and future studies in this rare tumor type.

Introduction

The recent integration of DNA methylation profiling of tumors of the central nervous system (CNS) has considerably improved diagnostic accuracy[1]. As a result, several newly defined tumor types have been included in the 5th edition of the WHO Classification of CNS Tumors[2–5]. 'Astroblastoma, *MN1*-altered' (ABM-*MN1*), originally designated as CNS high-grade neuroepithelial tumor, *MN1*-altered (HGNET-*MN1*), is a newly recognized and molecularly defined tumor type occurring in children, adolescents and young adults[6]. Tumors are characterized by specific gene fusions between the transcriptional regulator Meningioma 1 (*MN1*) proto-oncogene and the BEN domain containing 2 (*BEND2*) gene, or in some rare cases to the CXXC finger protein 5 (*CXXC5*) gene[2–4,6]. More recently, *EWSR1::BEND2* fusions were also described[7] in tumors classified by DNA-methylation as ABM-*MN1,* but it is currently unknown how they relate to ABM-*MN1* with *MN1* fusions[2].

Small retrospective series have reported a median age at presentation of 14 years, frequent supratentorial locations, and strong female predominance. Patients appear to have a relatively favorable overall survival, albeit relapses are frequently observed[6-16]. However, due to the rarity and recent description of this tumor type, large studies focusing on comprehensive in-depth analyses of clinical and molecular characteristics are lacking, resulting in a critical void in our understanding of effective therapeutic approaches.

To address this knowledge gap, we assembled a cohort of 200 patients with tumors classified as 'Astroblastoma, *MN1*-altered '(ABM-*MN1*), based on DNA methylation data and automated CNS tumor class prediction (https://www.molecularneuropathology.org/mnp/). Herein, we

describe the molecular, histopathological, and clinical features for this heterogeneous tumor type.

Materials and Methods

Patient Cohort and Study design

Due to the rarity of this tumor type, an extensive global collaboration was required. The overall study cohort and analyses are summarized as consort diagram in the supplementary material (Figure S1). To assemble a comprehensive cohort of Astroblastoma cases, we leveraged DNA methylation data from the Heidelberg methylation classifier (version 12.8) and the National Cancer Institute (NCI)/Bethesda classifier (version 1). Tumors classified as “Astroblastoma, *MN1*-altered” (ABM-MN1) or “NET-CXXC5” with calibrated scores >0.9 by either classifier were included. In parallel, additional cases harboring *MN1::BEND2*, *EWSR1::BEND2*, or *MN1::CXXC5* gene fusions were identified through collaborative contributions, previously published case reports, and smaller published cohorts[6–21]. Tumor specimens and associated molecular and clinical data were obtained from collaborating institutions and literature sources to build a robust multicenter dataset.

The study was approved by the ethics committees of all participating institutions, in accordance with the Declaration of Helsinki.

DNA methylation profiling

DNA was isolated from tumor samples, and DNA methylation profiling was performed using Illumina Human Methylation 450k or 850k/EPIC BeadChip arrays. DNA methylation and copy number calling were performed as described in previous studies[3,22–25].

Unsupervised Clustering Analyses

To investigate epigenetic heterogeneity, unsupervised clustering was performed using *t*-distributed stochastic neighbor embedding (*t*-SNE). A total of 200 tumor samples were included for analysis (Supplementary Table 1).

Histopathology Review

For histopathological review digital slides were reviewed by an experienced neuropathologist (K.A.) and scored with respect to distinct morphological features and expression of antigens.

RNA sequencing, gene expression profiling and DNA sequencing

RNAs isolated from tumor samples and with sufficient quality were further processed by RNA-sequencing (Illumina HiSeq4000) and gene expression profiling (Affymetrix GeneChip™ Human Genome U133Plus2.0), both performed by the DKFZ Genomics and Proteomics Core Facility. Fusions were called and analyzed based on RNA-seq data using Arriba (https://github.com/suhrig/arriba).

To identify other recurrent somatic mutations in our cohort, we integrated results from previous studies[6], molecular pathology reports and from new data generated with DNA gene panel sequencing performed at the Neuropathology department of the University Hospital Heidelberg.

Details of molecular analyses are outlined in the supplementary materials.

Clinical data and survival analyses

Demographics, disease characteristics, treatment and survival data were collected from contributing centers, and published data[7,8,30,31], and analyzed to perform clinico-molecular

correlations. To identify associations between molecular sub-types and clinical variables we used the Pearson's chi-square test. Overall Survival (OS) was defined as time from diagnosis until date of disease-related death or of last contact; Progression-free survival (PFS) was defined as time from diagnosis until first progression, relapse, death or date of last contact. Kaplan-Meier estimates and log-rank analyses were utilized to evaluate the impact of clinical, molecular features and therapeutic interventions. To identify clinical or molecular prognostic factors, we performed a univariate and multivariate cox proportional hazard analysis to estimate hazard ratios and 95% confidence intervals. All analyses were performed using SPSS (IBM, version 28). *P*-values below 0.05 were considered significant. Survival analyses and Kaplan-Meier illustrations were generated and performed using Graph Pad Prism.

Results

DNA methylation profiling identifies three groups within Astroblastoma, *MN1*-altered tumors defined by characteristic gene fusions

To investigate the molecular heterogeneity of tumors classified as ABM-*MN1* (Supplementary Figure S1), we performed DNA methylation-based *t*-SNE analyses on 200 tumors and compared the clustering with the reference set[6, 32]. All tumors in our cohort clustered distinctly from reference tumor entities (Figure 1A,B). Within the ABM-*MN1* cohort, independent methods including cola partitioning and unsupervised hierarchical clustering analyses supported identification of subgroups (Supplementary Figure S2A,B, see *Supplementary Methods*). To explore this further, we restricted *t*-SNE analysis to the 200 samples and correlated subgroups with available gene fusion data (Figure 1C,D; Supplementary Figure S3A,B).

Two main clusters were identified. The largest ABM-*MN1* cluster (n=180), segregated into two epigenetically related subgroups: Group A (n=143) and Group B (n=37) (Figure 1C-E), as

confirmed by cola partitioning analysis (Supplementary Table 1, Figure S2). Subgroups correlated with specific fusions in a mutually exclusive manner. Group A characteristically harbors *MN1::BEND2* fusions (n=22) or other *MN1* rearrangements (n=23), while validated *EWSR1::BEND2* fusions (n=7) and *EWSR1* rearrangements (n=1) were exclusively observed in Group B (Supplementary Figure S3B)[7]. In Group B we also identified two cases exhibiting a *MAMLD1::BEND2* fusion, indicating that alternative *BEND2*-fusion partners can be present in this group of tumors as well (Supplementary Figure S2B,C). A smaller cluster (Group C; n=20), consistently classified as NET-*CXXC5* by the latest DKFZ/Heidelberg classifier version, included all cases with *MN1::CXXC5* fusions (n=5) (Supplementary Figure S3B).

Taken together, DNA methylation profiling and clustering analyses indicated three distinct tumor groups that we annotated as “Group A” (143/200, 72%), “Group B” (37/200, 18%) and “Group C” (20/200, 10%), respectively (Figure 1E).

Breakpoint analysis revealed a consistent *MN1* breakpoint (in exon 1) when partnering to *BEND2* or *CXXC5* with a common breakpoint (in exon 2) for *CXXC5* (Supplementary Figure S3C). In contrast, *BEND2* demonstrates different breakpoint regions across four fusion types involving exons 6-14 (“fus1”), 7-14 (“fus2”), 8-14 (“fus3”), and 9-14 (“fus4”). As previously described by Lucas *et al*.[7], the *EWSR1::BEND2* typically involves exon 1-8 of *EWSR1* fused to exon 2-14 of *BEND2* or, less commonly, *EWSR1* exon 1-7 fused to *BEND2* exon 4-14.

Astroblastoma groups are histopathologically similar

Next, we evaluated the histological heterogeneity of this cohort, first by analyzing original institutional histological diagnoses available in 152 tumors. Overall, a variety of different diagnoses were originally assigned, including (anaplastic) astroblastoma (54/152, 36%), ependymoma (37/152, 24%), CNS-PNET (17/152, 11%), or other (44/152, 29%) (Figure 2A). These historic diagnoses slightly differed between the three molecular groups. In Group A, 46/111 (41%) tumors were originally diagnosed as (anaplastic) astroblastoma, compared to

only 7/26 (27%) tumors in Group B and 1/15 (7%) in Group C (Figure 2A). In contrast, ependymoma was the originally assigned diagnosis in 14/26 (54%) of tumors in Group B, while only accounted for 20/111 (18%) and 3/15 (20%) in Group A and C, respectively. High-grade glioma (HGG) was originally diagnosed in a relevant number of cases in Group C (4/15, 27%). Figure 2B shows exemplary hematoxylin and eosin (H&E) sections for each ABM subgroup, along with the original histopathological diagnoses.

For more detailed analyses, we performed histological evaluation on 36 available samples (Group A: n=24; Group B: n=8; Group C: n=4) by checking morphological features and performing immunostainings for Ki67, GFAP and OLIG2. No major differences were observed between the three groups for any of the histological features or immunostainings examined (Supplementary Figure S4). All tumors exhibited a circumscribed growth pattern, with no cases showing diffuse infiltration or entrapped axons. Astroblastic rosettes were present in 12/24 (50%) of Group A, 6/8 (75%) of Group B tumors, and 2/4 (50%) of Group C. Collagenous stroma was observed more frequently in Groups A (20/24, 83%) than in Group B (3/8, 38%) and Group C (2/4, 50%) (p=0.034).

Altogether, the histopathological analyses show that the three groups are highly related and belong to the same tumor type, but an integrated molecular and histopathological diagnosis is required for correct classification.

Chromosome X instability and recurrent copy number losses reveal molecular diversity

Analyses of chromosomal copy number alterations revealed significant instability of chromosome X in Group A tumors (119/143, 83%). This was less commonly observed in Group B tumors (14/37, 38%) and completely absent in Group C.

Among Group A tumors, partial or complete loss of one X chromosome (85/143, 59%) or chromothripsis of chromosome X (27/143, 19%) were the most frequent X-chromosome-related alterations (Figure 3A; Supplementary Figure S5A-C, S5E; Supplementary Table 2). In

addition to chromosome X instability, Group A tumors frequently showed characteristic losses of chromosomal arms 14q (23/143, 16%) and 16q (25/143, 17%). In this group, tumors with 16q loss tended to co-cluster in *t*-SNE analyses (Supplementary Figure S5C-D; Supplementary Table 2). Chromosomal copy number gains were less common and only detected in Group A, involving chromosome 1q (7/143, 5%), chromosome 5 (3/143, 2%) and chromosome 13 (4/137, 3%). In Group B, the most prominent alterations identified were losses of chromosome 10p (4/37, 11%) and 10q (6/37, 16%). In Group C, recurrent chromosome 11p losses (3/20, 15%) were observed (Figure 3A and Supplementary Figure S5B).

Transcriptional profiling reveals group-specific marker genes

We next analyzed transcriptome data to investigate how these three groups differ at the transcriptional level. Gene expression data was available for 27 samples, of which 23 had matching DNA methylation data (Group A n=14, Group B n=4, and Group C n=5). Clustering of the transcriptome data confirmed the methylation-assigned group annotation. In four cases without methylation data, clustering analyses assigned them to Group A.

As expected, we observed overexpression of group-specific fusion genes (Figure 3B). Differential gene expression analyses corroborated methylation results: Group A and B are transcriptionally related, while Group C showed a distinct gene expression signature (Figure 3C and Supplementary Table 2).

Group A tumors exhibited upregulation of genes involved in epithelial-mesenchymal transition and neural crest migration, such as *ABCC1*, *DLX5*, *PDGFRA*, *KITLG*, *COL4A1/2,* and *FZD2*. In contrast, samples from Group B demonstrated upregulation of *MUC1* (involved in glioblastoma progression[33]) and *KCNMB4*. Group C tumors showed high expression of fibroblast growth factors *FGF4 and FGF19*, *PAX5* previously described as a promoter of progression of astrocytomas to their malignant form[34], and several markers of neuronal development and differentiation (*SHC3*, *DCX*, *EFNA5, CNTN1*). Gene set enrichment

analyses revealed that the *NOTCH* signaling was enriched in Group A and *KRAS* oncogenic pathways predominated in Group C (Figure 3C,D and Supplementary Table 2).

In line with the striking female predominance observed in Group A (Figure 4A), we examined the expression of *XIST*, a non-coding RNA that mediates X chromosome inactivation. Moreover, *XIST* interaction with autosomal genes can lead to sex-specific unbalancing[35]. As expected, *XIST* was found to be upregulated in Group A tumors (Supplementary Table 2). To evaluate Group A-specific oncogenic mechanisms associated with *XIST*, we identified genes inversely correlated with *XIST* expression in Group A (Pearson correlation cut-off: <-0.7; p-value: <0,5) We identified 239 genes, including known tumor suppressor genes (*CDKN3*, *SDHD*), genes involved in the regulation of the cell cycle, DNA replication, cell differentiation, and morphogenesis, such as *SAPCD2*, *CCNA1*, *AURKA,* and *NEK2* (Supplementary Table 2). Interestingly, that correlation was absent in female patients from Group B, and other brain tumor entities without female predominance (data not shown).

Additionally, Group A and C demonstrated preferential expression of genes uniquely or predominantly detected in the cerebral cortex, including *UMODL1*, *TKTL1*, *ISLR2*, and *BCL11B* (Supplementary Table 2). In contrast, *HOXB2/3/4,* genes usually restricted to the human spinal cord (source: Human Protein Atlas; proteinatlas.org) were overexpressed in Group B tumors (Supplementary Table 2).

Finally, when integrating the ABM transcriptomic data with RNA data from other CNS tumor entities, we observed that Group A, B, and C marker genes were overrepresented compared to other brain tumor types. Amongst these genes, *ABCC1* (Group A), *MUC1* (Group B), *FGF3* and *FGF4* (Group C), were selectively overexpressed compared to normal brain. Importantly, these group-specific genes, along with *PDGFRA* (highly expressed in Groups A and B), have been predicted to be strong clinically actionable targets, according to DGIdb database[36] (Figure 3E-G and Supplementary Table 2).

Finally, integrated differentially methylated and expression analyses revealed that genes like *UMODL1* (Group A-enriched) and *CXXCL5* (Group C-enriched) displayed concordant

deregulation at both epigenetic and transcriptional levels (Supplementary Figure S5F,G), suggesting epigenetic regulation of group-specific gene marker expression.

Concurrent genomic alterations of ABM groups

We further examined the mutational landscape of ABM-*MN1* by analyzing recurrence of other mutations using previous whole-genome sequencing (WGS)/single nucleotide extension assay datasets[6], and additional panel sequencing data. Among 22 tumors with sequencing data, no highly recurrent alterations were identified. Still, a subset of genes , including *TSC2* (3/22), *NF1* (2/22), *PIK3C2B* (2/22), *NOTCH2* (2/22), and *KMT2C*, with the Y987H mutation (2/22) described in astrocytoma[37], were found mutated in more than one sample (Supplementary Figure S6A).

In line with breakpoints involving *MN1* on chromosome 22, frequent copy number losses involving *NF2* (n=15/200) and *SMARCB1* (n=5/200) were observed. In addition, we detected in a few cases *CDKN2A/B* focal deletions (n=4/200), and focal amplification in *EGFR* (n=2/200), *CDK4* (n=1/200), and *CCND1* (n=1/200) (Supplementary Figure S6B and Supplementary Table 2).

Astroblastoma groups show distinct patient characteristics

The age at diagnosis for the entire cohort ranged from very young to adult patients (range 0–48 years; median 11 years), with no major differences observed between the three groups: median age of 12, 7 and 11 years for Group A, Group B and Group C, respectively (Supplementary Figure S7A).

In the 5th edition of the WHO Classification of CNS Tumors ABM-*MN1* is described with a female predominance[2,5]. We found that this bias is entirely driven by Group A tumors, which

almost exclusively occur in female patients (139/143, 97%). In contrast, Groups B and C showed a slight male predominance (Figure 4A-C).

Tumor location significantly differed between the groups. Group A tumors were predominantly (96/98, 98%) and Group C tumors exclusively located supratentorially (10/10, 100%). In contrast, Group B tumors mostly presented in the spinal cord (11/22, 50%) and infratentorial regions of the brain (8/22, 36%), with only 3/22 (14%) located supratentorially (Figure 4D-F).

Astroblastoma groups impact clinical outcome

Clinical outcome and therapeutic data were available for 105 patients. Group B was associated with a significantly poorer prognosis, with a median PFS 1.3 years (95% CI 0–2.8 years) and median OS of 12.8 years (95% CI: not defined) (Figure 5A-B). In contrast, Group A median PFS was 4.3 years (95% CI: 1.8–6.8 years) and Group C median PFS was 5.1 years (95% CI: not defined). Despite frequent recurrences, overall survival was favorable for both groups, with 10-year OS rates of 89%.

Univariate cox proportional hazard analyses identified spinal location as an independent predictor of worse outcome; patients with spinal tumors were 3.69 times more likely to experience disease progression and 5 times more likely to die of their disease (PFS HR 3.69, 95% CI: 1.74–7.8; OS HR 5.12, 95% CI: 1.33–19.67). Group B itself was also a predictor of poor outcome (PFS HR 2.44, CI 1.32–4.52; OS HR 4.28, CI 1.30–14.13). Consistent with the predominance of spinal tumors in Group B, no independent association with inferior outcome was determined for spinal location (PFS HR 2.41, CI 0.79–7.37; OS HR 2.29, CI 0.36–14.35) or Group B (PFS HR 1.58, CI 0.61–4.07; OS HR 2.83, CI 0.57–14.10) upon multivariate analysis. Age at presentation, sex or tumor staging were not identified as independent predictors of outcome (Figure 5C).

Patterns of relapse varied across subgroups. Patients in Group C exclusively experienced local relapses (4/4, 100%), similarly, the majority of relapses in Group A were also local (29/38,

76%). In contrast, 6/15 (40%) of patients in Group B, showed new metastatic lesions in the CNS, distant to the primary tumor (Supplementary Table 1, Supplementary Figure S7B).

Treatment approaches were heterogeneous in keeping with the large variation of primary diagnoses. Most (61/84, 73%) patients, for which data was available, underwent gross-total resection (GTR) at initial surgery. Twenty-nine percent of patients (29/100) were managed with radiological surveillance (Supplementary Figure S8A-C). Upfront adjuvant treatment was applied to 71/100 (71%) patients and consisted of radiotherapy, given either alone (20/100, 20%) or in combination with chemotherapy (38/100, 41%), or chemotherapy alone (13/100, 10%).

A univariate cox proportional hazard analysis was utilized to understand the impact of individual therapeutic interventions for Group A and B. Group C was considered too small to interrogate therapeutic effects and it was excluded from this analysis. For Group A, GTR, chemotherapy or radiotherapy failed to demonstrate significant survival advantage (Figure 6A, 6C-D). Importantly, radiological observation was not associated with worse survival (Figure 6A). In Group B, however, upfront radiation therapy was associated with improved PFS (HR 0.25, CI 0.06–1.01, Figure 6B,E,F) but did not significantly improve OS. Spinal tumor location was also associated with worse prognosis in Group B alone (PFS HR 3.65, CI 0.93–14.39, Figure 6B).

Finally, we investigated the impact of CNVs on survival to identify prognostic biomarkers in Group A, our most robust subgroup. We identified that a combined loss of chromosomes 14q and 16q was associated with a significantly shorter PFS and OS, thereby representing the first identified molecular high-risk biomarker for this group. In contrast, alterations involving chromosome X did not impact survival outcomes (Supplementary Figure S9A-D).

Discussion

Our study shows that Astroblastoma, currently designated as “Astroblastoma, *MN1*-altered”, comprises three molecularly and clinically distinct groups, defined by characteristic gene fusions: *MN1::BEND2* (Group A), *EWSR1::BEND2* (Group B), and *MN1::CXXC5* (Group C). Rare cases with *MAMLD1::BEND2* fusions, or the recently reported *FUS::BEND2* and *TCF3::BEND2* fusions[38–40], also cluster with Group B. Based on our findings and the fact that not all tumors harbor *MN1* alterations, we propose renaming this tumor type as Astroblastoma. Because these tumors do not consistently present as glial neoplasms with astroblastic perivascular pseudorosettes and lack reliable IHC surrogate markers, molecular analyses are generally required to establish a diagnosis of astroblastoma. We recommend either DNA methylation profiling or detection of one of the characteristic gene fusions by sequencing as essential diagnostic criteria to support a correct classification of these tumors. These recommendations may be refined as further gene fusions within this group are identified.

Molecular analyses revealed that Group A and B are distinct but closely related at epigenetic and transcriptomic levels, while Group C has a more distinct methylation and gene expression profile as also recognized in the latest Heidelberg brain tumor classifier. Similar to NET-*PATZ1* tumors[32] where *MN1* and *EWSR1* are fusion partners of *PATZ1*, fusion proteins retain the transactivating domains of *MN1* and *EWSR1*[32,41–43], fused to the C-terminal domain of *BEND2*, containing two BEN domains, which is DNA binding[43]. This suggests that the oncogenic effect of the fusion proteins is determined by the transactivating capacity of *MN1* or *EWSR1* at respective *BEND2* binding sites.

Transcriptome analyses identified potential diagnostic and therapeutic biomarkers of clinical significance. For instance, *BEND2* was highly expressed in Group A and B, but not in other CNS brain tumor entities, suggesting its utility as a potential diagnostic marker. The *ABCC1* gene, overexpressed in Group A, encodes for the multidrug resistance protein 1 (*MRP1*), a known mediator of chemotherapy resistance in glioma[44–46], and may represent a target to increase chemotherapy sensitivity in these tumors. *MUC1*, upregulated in Group B, has been linked to glioma progression and regulation of oncogenic pathways[33,47,48]. In Group C we

identified *FGF4* highly expressed relatively to other CNS tumors, providing an additional potential diagnostic marker specific to this subgroup. Importantly, we also identified several potential therapeutic vulnerabilities, including PDGFRA, a receptor tyrosine kinase, highly overexpressed in Group A and B, and for which brain penetrant inhibitors have been developed[49]. Whether these tumors indeed respond to PDGFRA inhibitors needs validation in preclinical models, which are not readily available for these tumors.

Clinical features are distinct between the three groups, including sex distribution, tumor location and outcome. To our best knowledge, there is no other known brain tumor type like ABM Group A that affects almost exclusively females and the reasons for this are unclear. The non-coding RNA *XIST* may have a role in this by inactivating tumor suppressor genes that are only relevant in the context of *MN1::BEND2* fusions in Group A tumors. Future studies with genetically engineered mouse models overexpressing these *MN1::BEND2* fusions in the forebrain of male and female mice may shed more light on this, also whether female hormones may have an additional role in this.

In this study, we identified Group B as a high-risk subgroup, associated with a poor survival, high incidence of spinal tumors and frequent distant metastatic relapses, as suggested in previous single case reports[7,31]. Furthermore, our data suggest these patients may benefit from upfront radiotherapy. In contrast, Group A patients, demonstrated favorable outcomes after GTR, supporting a “watch and wait” strategy for patients with completely resected tumors, as previously proposed by some academic groups[2,50] For patients with incomplete resections or high-risk molecular features, such as co-deletion of 14q and 16q, postoperative radiotherapy could be considered.

These data represent the most comprehensive dataset assembled to date for this rare brain tumor tumor type and provide the scientific rationale to design a global, risk-stratified therapeutic trial for astroblastomas.

Our study is limited by the rarity of this tumor type, the retrospective nature of our cohort, the heterogeneity of treatment approaches and the small numbers within some subgroups.

Nevertheless, the integrated biological and clinical analyses offer pivotal insights that will be validated in a prospective manner.

In conclusion, our findings underscore the molecular and clinico-pathological heterogeneity within the current tumor type “Astroblastoma, *MN1*-altered” and provide crucial diagnostic and therapeutic information to guide future treatment strategies. The identification of high-risk biomarkers and actionable therapeutic targets are pivotal for the development of novel treatment approaches in these tumors.

Statements and Declarations

Ethics

This study was performed in line with the principles of the Declaration of Helsinki. Approval was granted by the Ethics Committee of the Medical University of Vienna (Date 30.05.2023/No 1244/2016).

Funding

This work was supported by a PhD stipend from the DKFZ to FSH, by the “City of Vienna Fund for Innovative Interdisciplinary Cancer Research” (JG), the “Forschungsgesellschaft für Cerebrale Tumore” (JG), and the Brain Tumour Charity (MK, JG and KvH).

Conflict of Interest

J.G. is consultant, advisory board participant and received honoraria for Novartis, Roche, Rhythm Pharmaceuticals, and Ipsen (not relevant to this study). J.H. has received consulting fees, honoraria, or is advisory board member for Servier International, ECOR1, and Alexion Pharmaceuticals and received travel support from Cure Brain Cancer Foundation. M.Z. has received honoraria or travel support from Astra Zeneca and Ipsen. C.K. advisory board for Boehringer Ingelheim. S.M.P. consulting for Epignostix GmbH and BioSkryb. M.A. pathology review panel for Servier.

Authorship

Aniello Federico, Felix Schmitt-Hoffner, Adriana Fonseca, Katja von Hoff, Johannes Gojo, and Marcel Kool conceptualized the study, performed the main analyses and prepared the first draft of the manuscript. Molecular analyses were perfomed by Aniello Federico, Felix Schmitt-Hoffner, and Monika Mauermann. Data collection was performed by Aniello Federico, Felix Schmitt-Hoffner, Adriana Fonseca, Neal Geisemeyer, Martin Sill, Damian Stichel, Dominik Sturm, Ulrich Schüller, Katharina Bruckner, Arnault Tauziede-Espariat, Pascale Varlet, David Capper, Zied Abdullaev, Daniel Schrimpf, Florian Selt, Lane Williamson, Andrew M. Donson, Manila Antonelli, Evelina Miele, Matija Snuderl, Sebastian Brandner, Maria Łastowska, Jasper van der Lugt, Jens Bunt, Christof Kramm, Alexandra Kolenova, Aditya Raghunathan, Yelena Wilson, Lauren Weintraub, Jordan R. Hansford, Sabine Spiegl-Kreinecker, Barbara Aistleitner, Lorena Baroni, Michal Zapotocky, Vijay Ramaswamy, Andrey Korshunov, Barbara Jones, Mimi Kjaersgaard, Mariëtte E Kranendonk, Christine Haberler, Roger J. Packer, Natalie Jäger, Katja

von Hoff, Johannes Gojo, and Marcel Kool. Resources essential for the scientific work were provided by Andreas von Deimling, Felix Sahm, Kenneth Aldape, Stefan M. Pfister, Johannes Gojo, Marcel Kool. Online access to all the molecular data presented in this manuscript via the Astroblastoma data scope in the R2 platform was accomplished by Jan Koster. The draft of the manuscript was written by Aniello Federico, Felix Schmitt-Hoffner, Adriana Fonseca, Katja von Hoff, Johannes Gojo, and Marcel Kool and all authors commented on previous versions of the manuscript. All authors read and approved the final manuscript.

Data availability

Upon publication, methylation and transcriptomic data publicly accessible on the R2: Genomics Analysis and Visualization Platform (http://r2.amc.nl) with a dedicated data scope (https://r2platform.com/astro/).

References

1. Sturm D, Capper D, Andreiuolo F, et al. Multiomic neuropathology improves diagnostic accuracy in pediatric neuro-oncology. *Nat Med*. 2023;29(4):917-926. doi:10.1038/s41591-023-02255-1

2. Louis DN, Perry A, Wesseling P, et al. The 2021 WHO Classification of Tumors of the Central Nervous System: a summary. *Neuro Oncol*. 2021;23(8):1231-1251. doi:10.1093/neuonc/noab106

3. Capper D, Jones DTW, Sill M, et al. DNA methylation-based classification of central nervous system tumours. *Nature*. 2018;555(7697):469-474. doi:10.1038/nature26000

4. Pfister SM, Reyes-Múgica M, Chan JKC, et al. A Summary of the Inaugural WHO Classification of Pediatric Tumors: Transitioning from the Optical into the Molecular Era. *Cancer Discov*. 2022;12(2):331-355. doi:10.1158/2159-8290.CD-21-1094

5. *Central Nervous System Tumours: WHO Classification of Tumours*. 5th ed. World Health Organization; 2022:584.

6. Sturm D, Orr BA, Toprak UH, et al. New Brain Tumor Entities Emerge from Molecular Classification of CNS-PNETs. *Cell*. 2016;164(5):1060-1072. doi:10.1016/j.cell.2016.01.015

7. Lucas C-HG, Gupta R, Wu J, et al. EWSR1-BEND2 fusion defines an epigenetically distinct subtype of astroblastoma. *Acta Neuropathol*. 2022;143(1):109-113. doi:10.1007/s00401-021-02388-y

8. Baroni LV, Rugilo C, Lubieniecki F, et al. Treatment response of CNS high-grade neuroepithelial tumors with MN1 alteration. *Pediatr Blood Cancer*. 2020;67(12):e28627. doi:10.1002/pbc.28627

9. Chen W, Soon YY, Pratiseyo PD, et al. Central nervous system neuroepithelial tumors with MN1-alteration: an individual patient data meta-analysis of 73 cases. *Brain Tumor Pathol*. 2020;37(4):145-153. doi:10.1007/s10014-020-00372-0

10. Lehman NL, Usubalieva A, Lin T, et al. Genomic analysis demonstrates that histologically-defined astroblastomas are molecularly heterogeneous and that tumors with MN1 rearrangement exhibit the most favorable prognosis. *Acta Neuropathol Commun*. 2019;7(1):42. doi:10.1186/s40478-019-0689-3

11. Burford A, Mackay A, Popov S, et al. The ten-year evolutionary trajectory of a highly recurrent paediatric high grade neuroepithelial tumour with MN1:BEND2 fusion. *Sci Rep*. 2018;8(1):1032. doi:10.1038/s41598-018-19389-9

12. Łastowska M, Trubicka J, Sobocińska A, et al. Molecular identification of CNS NB-FOXR2, CNS EFT-CIC, CNS HGNET-MN1 and CNS HGNET-BCOR pediatric brain tumors using tumor-specific signature genes. *Acta Neuropathol Commun*. 2020;8(1):105. doi:10.1186/s40478-020-00984-9

13. Mhatre R, Sugur HS, Nandeesh BN, Chickabasaviah Y, Saini J, Santosh V. MN1 rearrangement in astroblastoma: study of eight cases and review of literature. *Brain Tumor Pathol*. 2019;36(3):112-120. doi:10.1007/s10014-019-00346-x

14. Petruzzellis G, Alessi I, Colafati GS, et al. Role of DNA methylation profile in diagnosing astroblastoma: A case report and literature review. *Front Genet*. 2019;10:391. doi:10.3389/fgene.2019.00391

15. Tauziède-Espariat A, Pagès M, Roux A, et al. Pediatric methylation class HGNET-MN1: unresolved issues with terminology and grading. *Acta Neuropathol Commun*. 2019;7(1):176. doi:10.1186/s40478-019-0834-z

16. Wood MD, Tihan T, Perry A, et al. Multimodal molecular analysis of astroblastoma enables reclassification of most cases into more specific molecular entities. *Brain Pathol*. 2018;28(2):192-202. doi:10.1111/bpa.12561

17. Shin SA, Ahn B, Kim S-K, et al. Brainstem astroblastoma with MN1 translocation. *Neuropathology*. 2018;38(6):631-637. doi:10.1111/neup.12514

18. Hirose T, Nobusawa S, Sugiyama K, et al. Astroblastoma: a distinct tumor entity characterized by alterations of the X chromosome and MN1 rearrangement. *Brain Pathol*. 2018;28(5):684-694. doi:10.1111/bpa.12565

19. Boisseau W, Euskirchen P, Mokhtari K, et al. Molecular Profiling Reclassifies Adult Astroblastoma into Known and Clinically Distinct Tumor Entities with Frequent Mitogen-Activated Protein Kinase Pathway Alterations. *Oncologist*. 2019;24(12):1584-1592. doi:10.1634/theoncologist.2019-0223

20. Neumann JE, Spohn M, Obrecht D, et al. Molecular characterization of histopathological ependymoma variants. *Acta Neuropathol*. 2020;139(2):305-318. doi:10.1007/s00401-019-02090-0

21. Yamada SM, Tomita Y, Shibui S, et al. Primary spinal cord astroblastoma: case report. *J Neurosurg Spine*. 2018;28(6):642-646. doi:10.3171/2017.9.SPINE161302

22. Capper D, Stichel D, Sahm F, et al. Practical implementation of DNA methylation and copy-number-based CNS tumor diagnostics: the Heidelberg experience. *Acta Neuropathol*. 2018;136(2):181-210. doi:10.1007/s00401-018-1879-y

23. Korshunov A, Okonechnikov K, Schmitt-Hoffner F, et al. Molecular analysis of pediatric CNS-PNET revealed nosologic heterogeneity and potent diagnostic markers for CNS neuroblastoma with FOXR2-activation. *Acta Neuropathol Commun*. 2021;9(1):20. doi:10.1186/s40478-021-01118-5

24. von Hoff K, Haberler C, Schmitt-Hoffner F, et al. Therapeutic implications of improved molecular diagnostics for rare CNS embryonal tumor entities: results of an international, retrospective study. *Neuro Oncol*. 2021;23(9):1597-1611. doi:10.1093/neuonc/noab136

25. Federico A, Thomas C, Miskiewicz K, et al. ATRT-SHH comprises three molecular subgroups with characteristic clinical and histopathological features and prognostic significance. *Acta Neuropathol*. 2022;143(6):697-711. doi:10.1007/s00401-022-02424-5

26. Okonechnikov K, Joshi P, Sepp M, et al. Mapping pediatric brain tumors to their origins in the developing cerebellum. *Neuro Oncol*. 2023;25(10):1895-1909. doi:10.1093/neuonc/noad124

27. Subramanian A, Tamayo P, Mootha VK, et al. Gene set enrichment analysis: a knowledge-based approach for interpreting genome-wide expression profiles. *Proc Natl Acad Sci USA*. 2005;102(43):15545-15550. doi:10.1073/pnas.0506580102

28. Liberzon A, Subramanian A, Pinchback R, Thorvaldsdóttir H, Tamayo P, Mesirov JP. Molecular signatures database (MSigDB) 3.0. *Bioinformatics*. 2011;27(12):1739-1740. doi:10.1093/bioinformatics/btr260

29. Blattner-Johnson M, Jones DTW, Pfaff E. Precision medicine in pediatric solid cancers. *Semin Cancer Biol*. 2022;84:214-227. doi:10.1016/j.semcancer.2021.06.008

30. Pagès M, Pajtler KW, Puget S, et al. Diagnostics of pediatric supratentorial RELA ependymomas: integration of information from histopathology, genetics, DNA methylation and imaging. *Brain Pathol*. 2019;29(3):325-335. doi:10.1111/bpa.12664

31. Tsutsui T, Arakawa Y, Makino Y, et al. Spinal cord astroblastoma with EWSR1-BEND2 fusion classified as HGNET-MN1 by methylation classification: a case report. *Brain Tumor Pathol*. 2021;38(4):283-289. doi:10.1007/s10014-021-00412-3

32. Alhalabi KT, Stichel D, Sievers P, et al. PATZ1 fusions define a novel molecularly distinct neuroepithelial tumor entity with a broad histological spectrum. *Acta Neuropathol*. 2021;142(5):841-857. doi:10.1007/s00401-021-02354-8

33. Kim S, Seo Y, Chowdhury T, et al. Inhibition of MUC1 exerts cell-cycle arrest and telomerase suppression in glioblastoma cells. *Sci Rep*. 2020;10(1):18238. doi:10.1038/s41598-020-75457-z

34. Stuart ET, Kioussi C, Aguzzi A, Gruss P. PAX5 expression correlates with increasing malignancy in human astrocytomas. *Clin Cancer Res*. 1995;1(2):207-214.

35. Dror I, Chitiashvili T, Tan SYX, et al. XIST directly regulates X-linked and autosomal genes in naive human pluripotent cells. *Cell*. 2024;187(1):110-129.e31. doi:10.1016/j.cell.2023.11.033

36. Freshour SL, Kiwala S, Cotto KC, et al. Integration of the Drug-Gene Interaction Database (DGIdb 4.0) with open crowdsource efforts. *Nucleic Acids Res*. 2021;49(D1):D1144-D1151. doi:10.1093/nar/gkaa1084

37. Shankar GM, Lelic N, Gill CM, et al. BRAF alteration status and the histone H3F3A gene K27M mutation segregate spinal cord astrocytoma histology. *Acta Neuropathol*. 2016;131(1):147-150. doi:10.1007/s00401-015-1492-2

38. Tauziède-Espariat A, Bonhomme B, Truffaux N, et al. A novel FUS::BEND2 fusion expanding the molecular spectrum of astroblastomas. *Free Neuropathology*. 2024;5:34. doi:10.17879/freeneuropathology-2024-5983

39. Nakano Y, Nobusawa S, Sato-Otsubo A, et al. TCF3::BEND2 in paediatric supratentorial tumour with carcinoma-like epithelial features classifying as MN1-altered astroblastoma by DNA methylation profiling. *Neuropathol Appl Neurobiol*. 2024;50(5):e13011. doi:10.1111/nan.13011

40. Zheng L, Luo T, Xian J, et al. A primary intracranial neuroepithelial neoplasm with novel TCF3::BEND2 fusion: a case report. *Acta Neuropathol Commun*. 2024;12(1):175. doi:10.1186/s40478-024-01884-y

41. Grünewald TGP, Cidre-Aranaz F, Surdez D, et al. Ewing sarcoma. *Nat Rev Dis Primers*. 2018;4(1):5. doi:10.1038/s41572-018-0003-x

42. Miyake N, Takahashi H, Nakamura K, et al. Gain-of-Function MN1 Truncation Variants Cause a Recognizable Syndrome with Craniofacial and Brain Abnormalities. *Am J Hum Genet*. 2020;106(1):13-25. doi:10.1016/j.ajhg.2019.11.011

43. Dai Q, Ren A, Westholm JO, Serganov AA, Patel DJ, Lai EC. The BEN domain is a novel sequence-specific DNA-binding domain conserved in neural transcriptional repressors. *Genes Dev*. 2013;27(6):602-614. doi:10.1101/gad.213314.113

44. Tivnan A, Zakaria Z, O'Leary C, et al. Inhibition of multidrug resistance protein 1 (MRP1) improves chemotherapy drug response in primary and recurrent glioblastoma multiforme. *Front Neurosci*. 2015;9:218. doi:10.3389/fnins.2015.00218

45. Chen Z, Zhang Y, Chen Y, et al. Prrx1 promotes resistance to temozolomide by upregulating ABCC1 and inducing vasculogenic mimicry in glioma. *Am J Cancer Res*. 2022;12(8):3892-3912.

46. Chen X-R, Zhang Y-G, Wang Q. miR-9-5p Mediates ABCC1 to Elevate the Sensitivity of Glioma Cells to Temozolomide. *Front Oncol*. 2021;11:661653. doi:10.3389/fonc.2021.661653

47. Lee Y, Flores CC, Lefton M, Bhoumik S, Owada Y, Gerstner JR. Integrated Transcriptome Profiling and Pan-Cancer Analyses Reveal Oncogenic Networks and Tumor-Immune Modulatory Roles for FABP7 in Brain Cancers. *Int J Mol Sci*. 2024;25(22). doi:10.3390/ijms252212231

48. Tong F, Zhao J-X, Fang Z-Y, et al. MUC1 promotes glioblastoma progression and TMZ resistance by stabilizing EGFRvIII. *Pharmacol Res*. 2023;187:106606. doi:10.1016/j.phrs.2022.106606

49. Mayr L, Trissal M, Schwark K, et al. Dddr-22. translation of the pdgfra/kit inhibitor avapritinib for pediatric high-grade glioma. *Neuro Oncol*. 2022;24(Supplement_7):vii103-vii103. doi:10.1093/neuonc/noac209.387

50. Gojo J, Kjaersgaard M, Zezschwitz BV, et al. Rare embryonal and sarcomatous central nervous system tumours: State-of-the art and future directions. *Eur J Med Genet*. 2023;66(1):104660. doi:10.1016/j.ejmg.2022.104660

Figure Legends

Figure 1. DNA methylation and clustering analyses unveiled three distinct epigenetic groups. (A-B) *t*-SNE analyses calculated on the top 2,500 variable probes of the DNA methylation data forming the cohort including the ABM, *MN1*-altered patient cases (n=200; highlighted in red in Figure 1A) and external references representing other CNS tumors (n= 614) derived from the analysis described in the study of Alhalabi *et al*. **(C)** *t*-SNE plot of ABM, *MN1*-altered cohort (n=200). Based on the results of unsupervised clustering analyses, this group of samples formed three stable subclusters: ABM Group A, ABM Group B and ABM Group C. **(D)** Reclustering on samples forming the main cluster observed in Figure 1C, highlighting the separation between Group A and Group B subclusters. **(E)** Proportions of the three ABM groups found in our cohort. Abbreviations of tumor entities as described in mnp v12.8 brain classifier: CNS_NB-*FOXR2*: CNS neuroblastoma with *FOXR2* activation; CNS_EFT-*CIC*: CNS ewing sarcoma family tumor with *CIC* alteration; CNS_HGNET-*BCOR*: CNS high-grade neuroepithelial tumor with *BCOR* alteration; HGNET_*PATZ1* neuroepithelial tumor with *PATZ1* fusion; HGG_G34: Diffuse pediatric-type high grade glioma, H3.3 G34 mutant; HGG_K27: Diffuse glioma, H3K27-altered; HGG_IDH: Diffuse glioma, IDH mutant; HGG_RTK: Diffuse pediatric-type high grade glioma, RTK subtype; HGG_*MYCN*: Diffuse pediatric-type high grade glioma, *MYCN* subtype; PXA: Pleomorphic Xanthoastrocytoma; AT/RT: Atypical teratoid rhabdoid tumor; CPC: Choroid Plexus tumor; DIG: Desmoplastic infantile ganglioglioma; EWS: Ewing sarcoma; MNG: Meningioma; ETMR: Embryonal tumor with multilayered rosettes; MB_SHH: Medulloblastoma, SHH-activated; MB_WNT: Medulloblastoma, WNT activated; MB_GRP3: Medulloblastoma Group 3; MB_GRP4: Medulloblastoma Group 4; PINEAL: pineal tumor; EPN_*ZFTA*: Supratentorial Ependymoma, *ZFTA* fusion-positive; EPN_*YAP*: Supratentorial Ependymoma, *YAP1*-fused; CTRL: Control brain tissue.

Figure 2. Spectrum of original institutional histological diagnoses. (A) Proportions of the various originally assigned histopathological institutional diagnoses reported for the patients forming our study cohort and in each of the ABM groups described in our study. **(B-D)** Exemplary histopathology images showing H/E stainings of two cases per group. Abbreviations: ABM: Astroblastoma; anapl. ABM: Anaplastic Astroblastoma; CNS-PNET: Central Nervous System Primitive Neuro-Ectodermal tumor, a historic diagnostic term for a heterogeneous group of tumors, which histopathologically appear as embryonal tumors. This term has discarded in the revised 4th edition of the WHO classification of tumors of the CNS in 2016 and is no longer appropriate, but was assigned to the tumors before 2016; EPN: Ependymoma; HGG: High-grade Glioma; MB: Medulloblastoma.

Figure 3. The ABM groups are characterized by distinct copy number alterations and transcriptomic profiles. (A) Chromosome-wide CNV heatmap of all the cases present in our DNA methylation cohort (n=200). Blue regions indicated chromosomal losses, while gains were reported in red. **(B)** Expression plot of the genes involved in *MN1*-fusion transcripts in Group A/B (*BEND2*) and Group C (*CXXC5*). **(C)** Gene expression heatmap and semi-supervised clustering analyses of our transcriptome cohort. The heatmap showed the expression values (log 2 Z-scores) of the differentially expressed genes across ABM groups. Functional markers have been highlighted. **(D)** GSEA analyses of Group A and Group C enriched gene signatures. **(E-F)** Volcano plots highlighting significant Group A-, Group B-, and Group C- upregulated genes compared with other ABM and CNS tumor entities.

Figure 4. Sex imbalance and variations in tumor location among the three groups. (A-C) Sex distribution amongst the ABM groups described in this study. **(D-F)** Representation of the original tumor location of the tumors enrolled in our study and then stratified based on the molecular groups.

Figure 5. Survival analyses revealed the prognostic value of ABM group stratification. (A-B) Progression-free and overall survival of astroblastoma groups plotted as Kaplan Meier curves. Median survival and 95% confidence interval are indicated. P-values in-between

groups were calculated by log-rank test. 2-year, 5-year and 10-year survival rates and 95% confidence intervals are indicated. **(C)** Univariate hazard ratios calculated for clinical and molecular parameters by cox proportional hazards model for progression-free and overall survival.

Figure 6. Risk assessment for ABM Group A and Group B patients in relation to their treatment regimen. (A-B) Univariate hazard ratios calculated for clinical parameters and therapeutic interventions within Group A and Group B by Cox proportional hazards model for progression-free and overall survival. **(C-D)** Kaplan-Meier curves of progression-free and overall survival for gross-total resection and irradiation in Group A. P-values were calculated by log-rank test. **(E-F)** Kaplan-Meier curves of progression-free and overall survival for gross-total resection and irradiation in Group B.

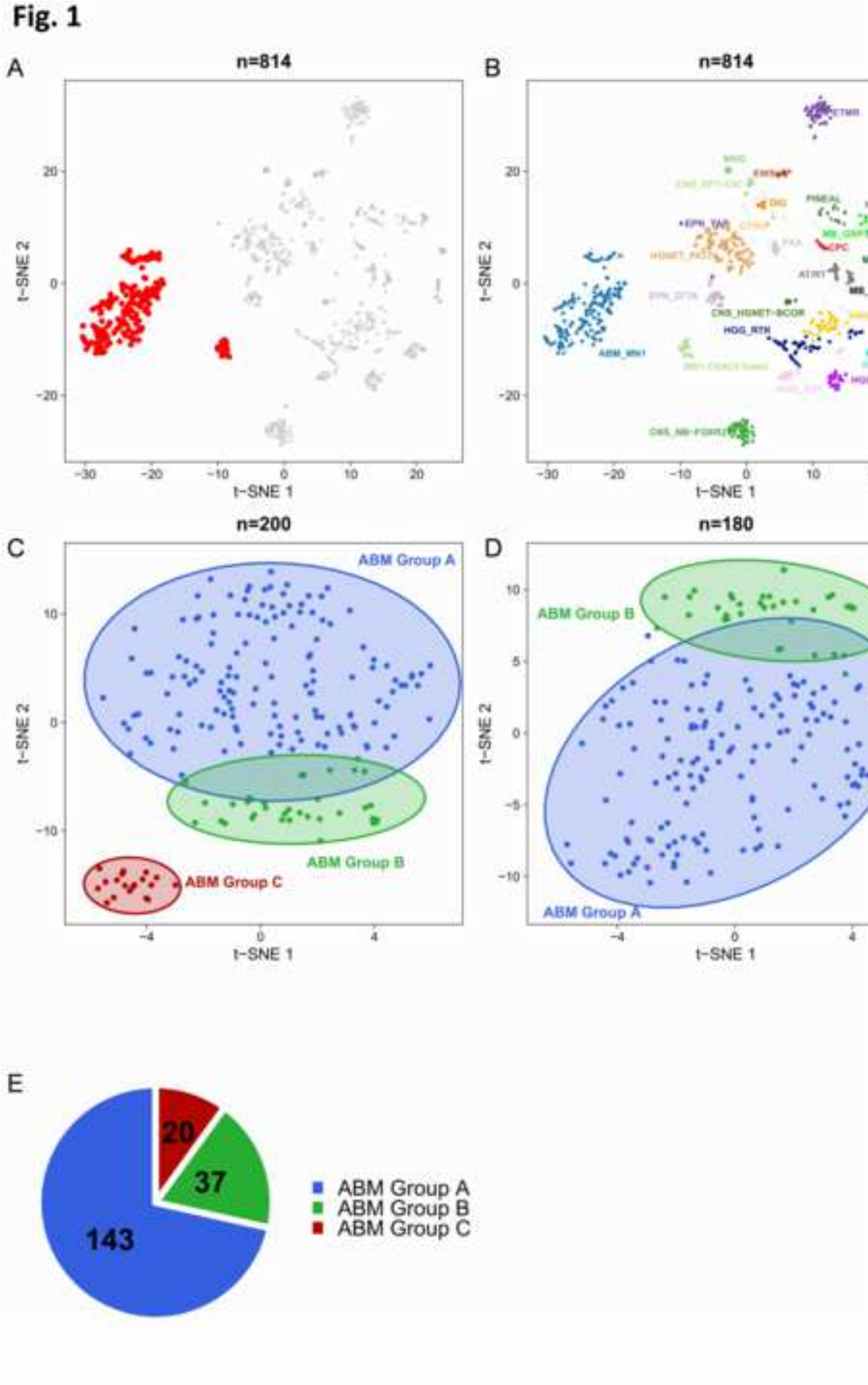

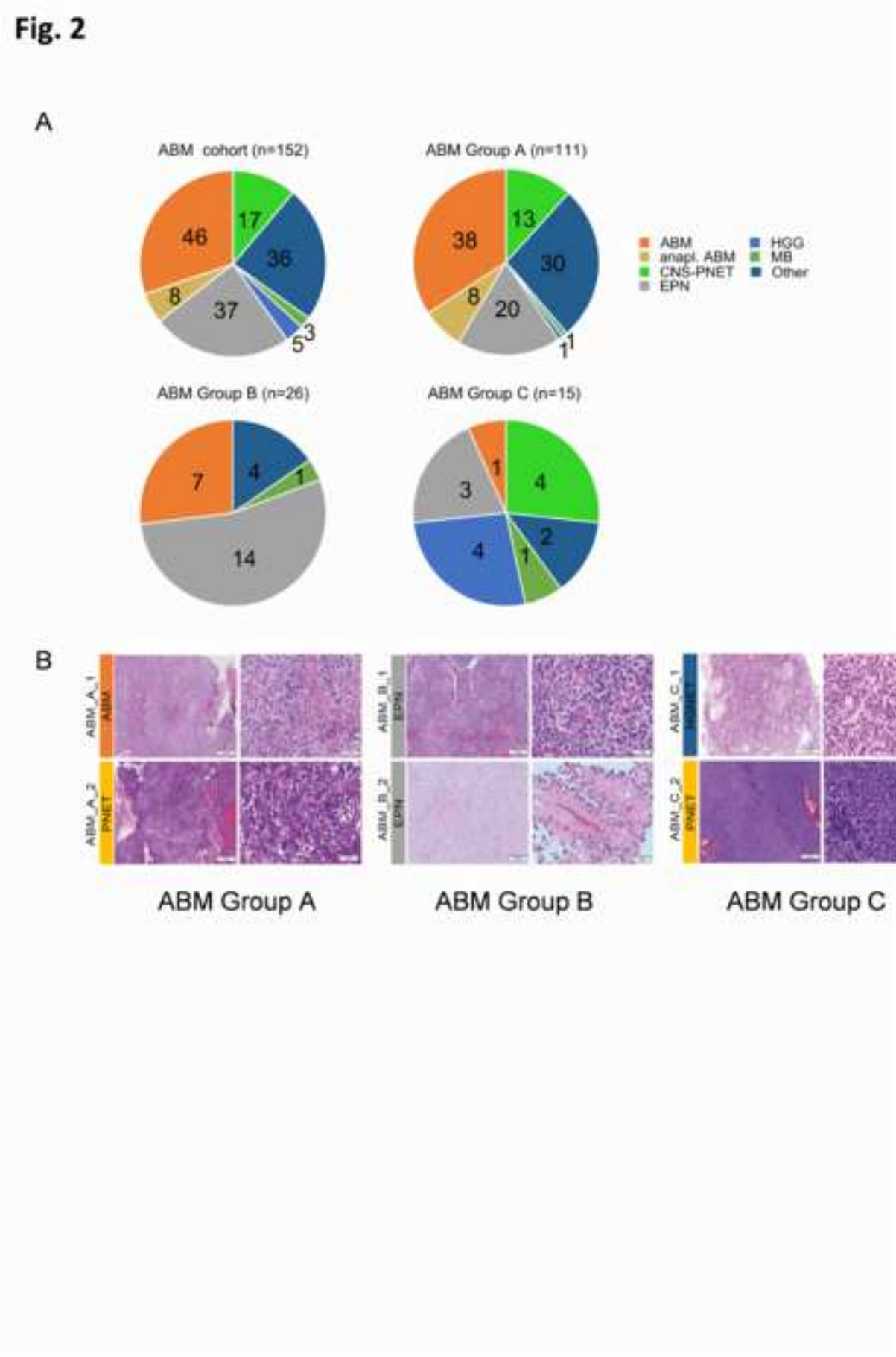

Fig. 3

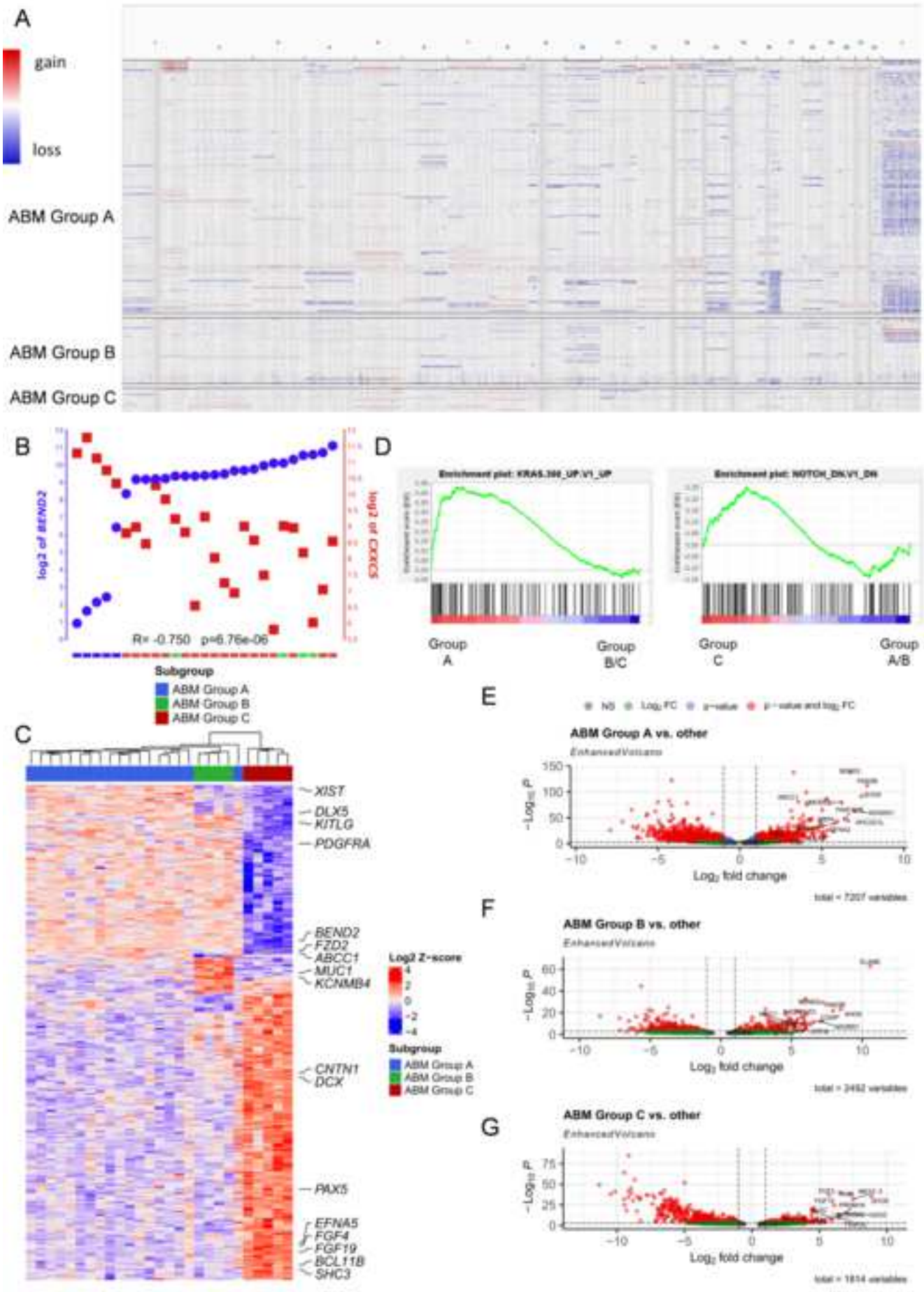

Fig. 4

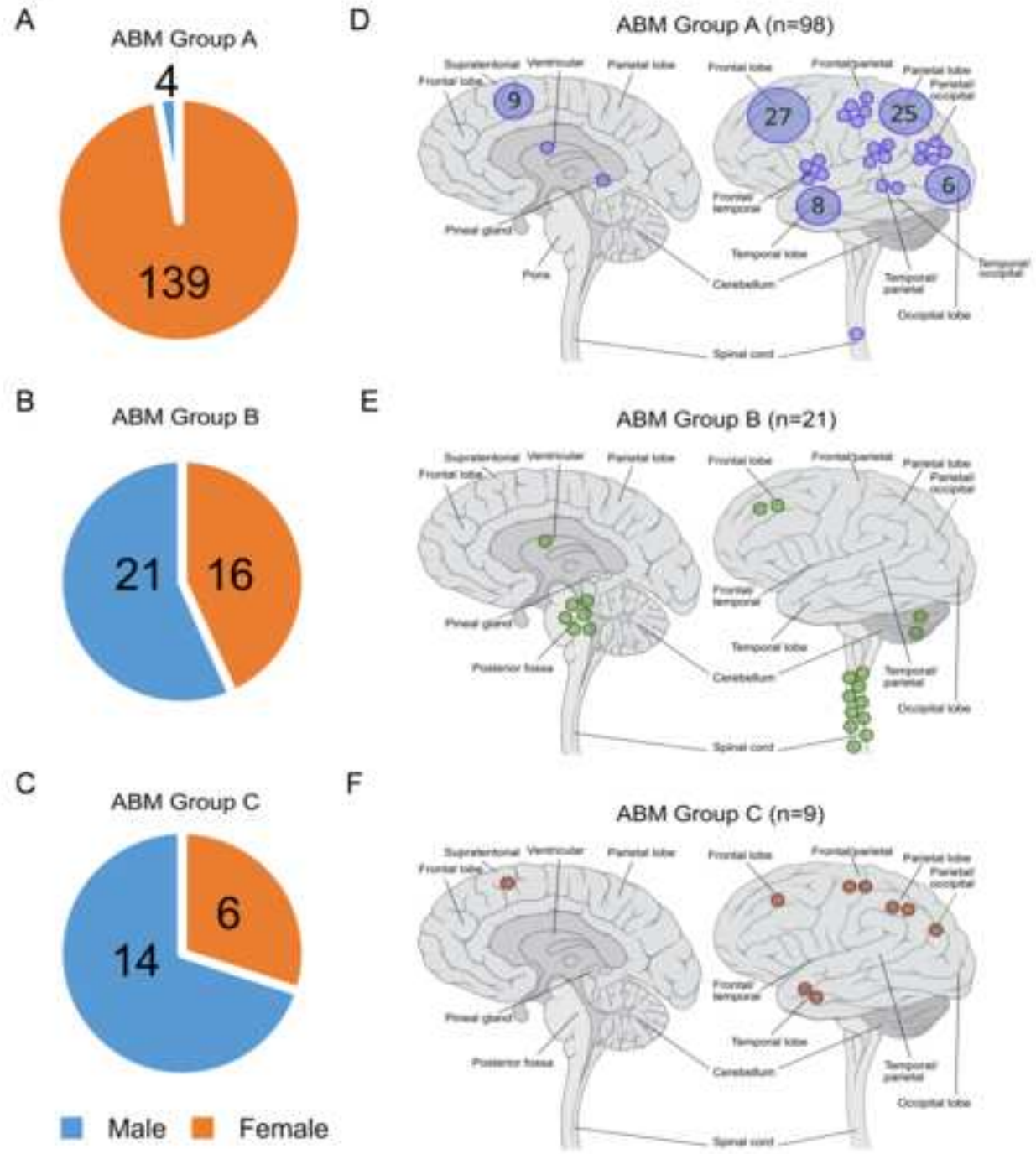

Fig.5

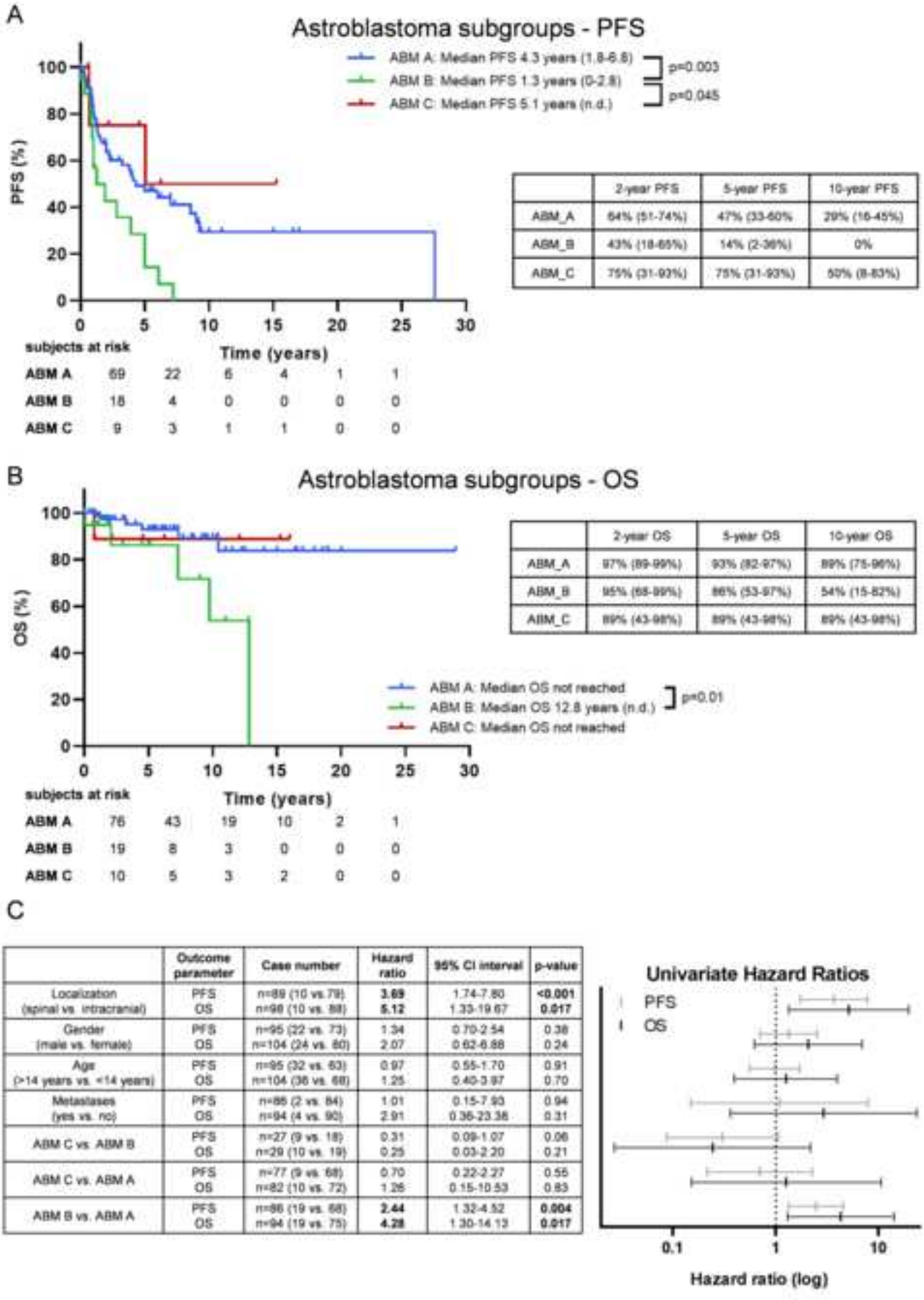

	2-year PFS	5-year PFS	10-year PFS
ABM_A	64% (51-74%)	47% (33-60%	29% (16-45%)
ABM_B	43% (18-65%)	14% (2-36%)	0%
ABM_C	75% (31-93%)	75% (31-93%)	50% (8-83%)

	2-year OS	5-year OS	10-year OS
ABM_A	97% (89-99%)	93% (82-97%)	89% (75-96%)
ABM_B	95% (68-99%)	86% (53-97%)	54% (15-82%)
ABM_C	89% (43-98%)	89% (43-98%)	89% (43-98%)

C

	Outcome parameter	Case number	Hazard ratio	95% CI interval	p-value
Localization (spinal vs. intracranial)	PFS OS	n=89 (10 vs.79) n=98 (10 vs. 88)	**3.69** **5.12**	1.74-7.80 1.33-19.67	**<0.001** **0.017**
Gender (male vs. female)	PFS OS	n=95 (22 vs. 73) n=104 (24 vs. 80)	1.34 2.07	0.70-2.54 0.62-6.88	0.38 0.24
Age (>14 years vs. <14 years)	PFS OS	n=95 (32 vs. 63) n=104 (36 vs. 68)	0.97 1.25	0.55-1.70 0.40-3.97	0.91 0.70
Metastases (yes vs. no)	PFS OS	n=86 (2 vs. 84) n=94 (4 vs. 90)	1.01 2.91	0.15-7.93 0.36-23.38	0.94 0.31
ABM C vs. ABM B	PFS OS	n=27 (9 vs. 18) n=29 (10 vs. 19)	0.31 0.25	0.09-1.07 0.03-2.20	0.06 0.21
ABM C vs. ABM A	PFS OS	n=77 (9 vs. 68) n=82 (10 vs. 72)	0.70 1.26	0.22-2.27 0.15-10.53	0.55 0.83
ABM B vs. ABM A	PFS OS	n=86 (19 vs. 68) n=94 (19 vs. 75)	**2.44** **4.28**	1.32-4.52 1.30-14.13	**0.004** **0.017**

Fig. 6

A

ABM A	Outcome parameter	Case number	Hazard ratio	95% CI interval	p-value
Extent of resection (GTR vs. non GTR)	PFS OS	n=52 (43 vs. 9) n=46 (10 vs. 36)	0.76 31.17	0.31-1.88 <0.1->10	0.55 0.55
RTX (yes vs. no)	PFS OS	n=63 (37 vs. 26) n=65 (38 vs. 27)	1.44 1.23	0.71-2.93 0.21-7.36	0.32 0.82
CTX (yes vs. no)	PFS OS	n=60 (33 vs. 27) n=62 (32 vs. 30)	1.63 4.31	0.80-3.35 0.48->10	0.18 0.19
Surveillance (yes vs. No)	PFS OS	n=66 (22 vs. 44) n=67 (22 vs. 45)	0.59 0.025	0.27-1.26 <0.001->10	0.17 0.35

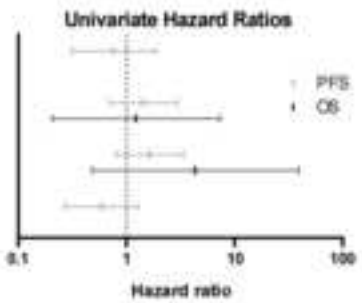

B

ABM B	Outcome parameter	Case number	Hazard ratio	95% CI interval	p-value
Extent of resection (GTR vs. non GTR)	PFS OS	n=17 (9 vs. 8) n=18 (10 vs. 8)	0.72 0.16	0.22-2.32 0.02-1.59	0.58 0.11
RTX (yes vs. no)	PFS OS	n=15 (11 vs. 4) n=16 (12 vs. 4)	0.25 <0.1	0.06-1.01 <0.1->10	0.05 0.60
CTX (yes vs. no)	PFS OS	n=13 (8 vs. 5) n=14 (9 vs. 5)	1.41 0.533	0.39-5.13 0.05-5.89	0.60 0.61
Localization (spinal vs. intracranial)	PFS OS	n=17 (10 vs. 17) n=18 (10 vs. 8)	**3.65** **4.76**	0.93-14.39 0.47->10	0.06 0.19

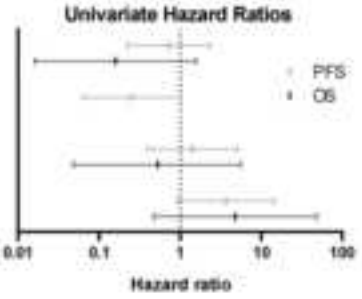

C

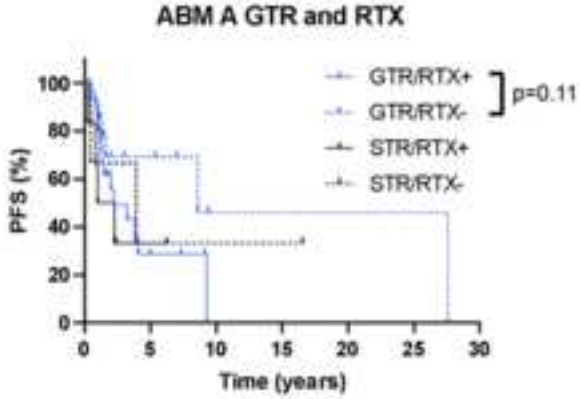

subjects at risk						
GTR/RTX+	26	4	0	0	0	0
GTR/RTX-	15	5	1	1	1	1
STR/RTX+	6	1	0	0	0	0
STR/RTX-	3	1	1	1	0	0

D

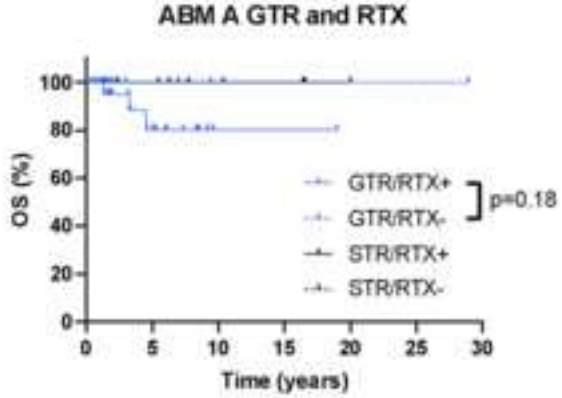

subjects at risk						
GTR/RTX+	26	10	1	1	0	0
GTR/RTX-	16	7	3	1	1	1
STR/RTX+	6	3	1	1	1	0
STR/RTX-	3	3	2	2	0	0

E

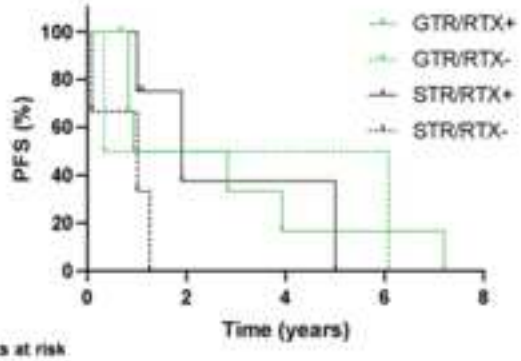

subjects at risk				
GTR/RTX+	7	3	1	1
GTR/RTX-	2	1	1	1
STR/RTX+	4	1	1	0
STR/RTX-	3	0	0	0

F

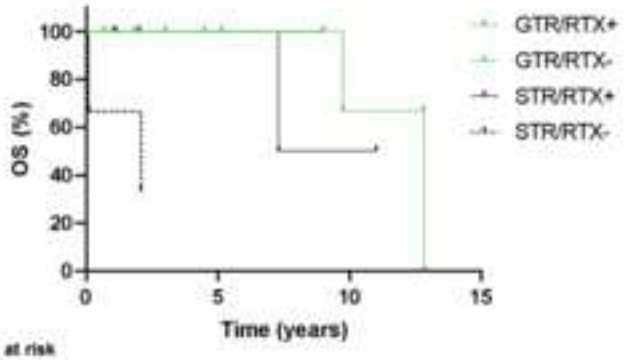

subjects at risk			
GTR/RTX+	8	4	2
GTR/RTX-	2	1	0
STR/RTX+	4	2	1
STR/RTX-	3	0	0

Graphical Abstract

Astroblastoma

Group	Astroblastoma Group A	Astroblastoma Group B	Astroblastoma Group C
Biological hallmark	***MN1::BEND2***	***EWSR1::BEND2*** + other rare *XX::BEND2* fusions (*XX* = *MAMLD1, FUS, TCF3*)	***MN1::CXXC5* fusion**
Transcriptome	*ABCC1, DLX5, KITLG, COL4A1/2, FZD2*	*MUC1, KCNMB4, HOXB2/3/4*	*PAX5, SHC3, DCX, EFNA5, CNTN1*
Copynumber aberrations	14q-, 16q-, Xp-, Xq- X chromothripsis	10p-, 10q- X chromothripsis	11p-
Oncogenic pathways	NOTCH, PDGFRA	PDGFRA	KRAS, FGFR
Demographics Gender Ratio (F:M) Median Age	  97% : 3% 12 years	  43% : 57% 7 years	  30% : 70% 11 years
Tumor location	 98% 2%	 14% 36% 50%	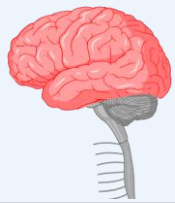 100%
Metastasis	3% at diagnosis 11% at relapse	0% at diagnosis 40% at relapse	no metastases observed
Progression-free survival	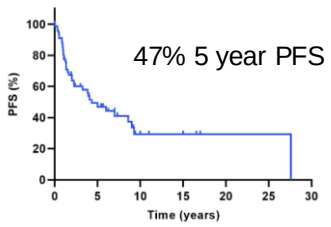	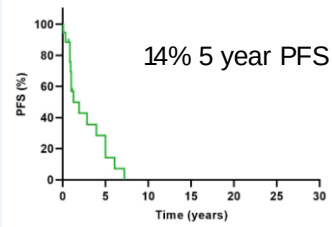	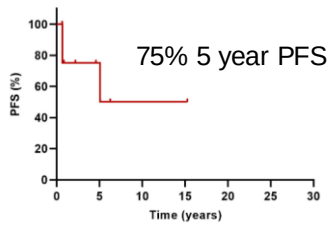
Overall survival	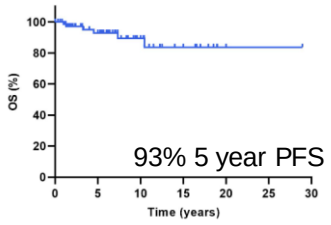	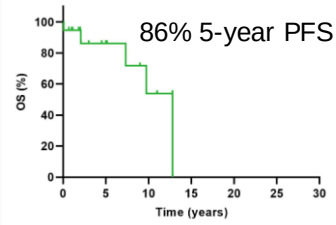	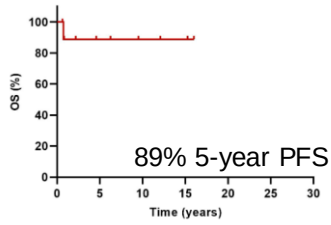
Risk factors	14q-, 16q-	Spinal location, no RTX	not known